

DEM Simulation of Soil Loosening Process Caused by a Vibrating Subsoiler

Hiroaki. Tanaka ^{1,*}, Akira. Oida ², Masamichi Daikoku ¹, Koji Inooku ³,
Osamu Sumikawa ⁴, Yuji Nagasaki ¹ and Masahiro Miyazaki ⁵

¹ National Agricultural Research Center for Western Region,
2575 Ikano, Zentsuji, Kagawa 765-0053, Japan.

² Professor Emeritus, Agricultural Systems Engineering Section,
Graduate School of Agriculture, Kyoto University, Kyoto 606-8502, Japan.

³ Bio-oriented Technology Research Advancement Institution, Saitama, Japan.

⁴ National Institute of Vegetable and Tea Science, Shizuoka, Japan.

⁵ National Agricultural Research Center, Ibaraki, Japan.

*E-mail: hirtana@affrc.go.jp

ABSTRACT

By using the distinct element method (DEM), a soil mechanical model was developed to simulate the soil loosening process caused by a vibrating subsoiler. This study focuses on the cracking of soil caused by the motion of the subsoiler shank. In the field experiment, the state of cracking was observed in a cross section of the field. In the DEM simulation, the mechanical relationship between elements was improved in order to represent a series of processes ranging from continuous to discontinuous behavior of soil, such as cracking and fracturing. The simulation result satisfactorily represented the failure plane, failure zone, and cracking of soil caused by the test subsoiler.

Keywords: Distinct element method (DEM), numerical simulation, soil cracking, failure plane, subsoiler shank, Japan.

1. INTRODUCTION

A vibrating wide subsoiler, which consists of two curved shanks and one straight shank, achieves subsurface tillage when attached to a 18.4-31.6 kW tractor. The uniqueness of this subsoiler lies in the shape and arrangement of the shanks, as shown in Figure 1. The curved shanks are arranged on both sides of a frame. The horizontal distance between them is adjustable. The straight shank is usually located at the center along with a chisel. The maximum operating width and depth of the subsoiler are 1.6 and 0.5 m, respectively. The surface of the ground is lifted 3–5 cm during the subsoiling process, and cracks appear in the cross section of the field.

Although this implement is commercially available, there is still a need to improve its performance by reducing the draft and improving the uniformity of soil loosening. This necessitates an in-depth study of the soil-tool interaction for effective subsoiling.

The dynamic soil behavior, particularly the motion of the soil in subsurface layers, is complex and hard to be observed directly. Therefore, numerical methods should be employed in order to predict

H. Tanaka, A. Oida, M. Daikoku, K. Inooku, O. Sumikawa, Y. Nagasaki and M. Miyazaki.
“DEM Simulation of Soil Loosening Process Caused by a Vibrating Subsoiler”. Agricultural
Engineering International: the CIGR Ejournal. Manuscript PM 05 010. Vol. IX. November,
2007.

the dynamic soil behavior and to evaluate the effect of subsoiling.

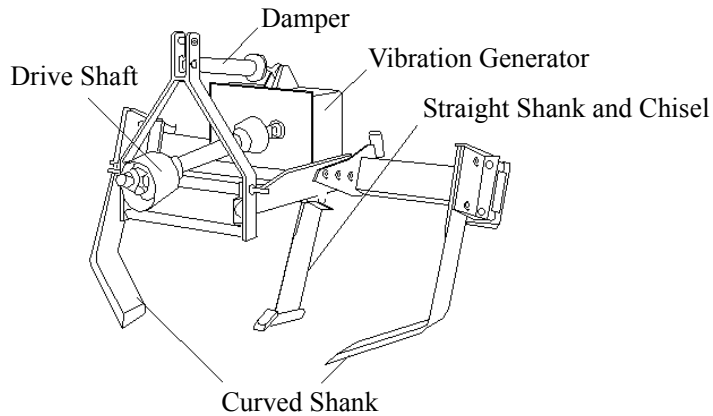


Figure 1. The vibrating wide subsoiler.

Thus far, the finite element method (FEM) has been widely applied to the analysis of the interaction between the soil and agricultural equipments such as tires and tillage tools. However, this method is difficult to be applied to problems of large-scale deformation, particularly in cases where the soil is cut and separated, because it is based on the continuum mechanics. Therefore, an appropriate method is required for simulating such problems.

The distinct element method (DEM) is one of the methods in computational mechanics, and it was originally proposed by Cundall and Strack (1979) to analyze the dynamic behavior of granular materials. This method has been applied in several fields such as soil mechanics, powder technology, and agricultural process engineering (Sakaguchi et al., 2001). In the field of terramechanics, there have been some reports on the application of the DEM to dynamic and large-scale problems of soil-machine interaction (Tanaka et al., 2000a, 2000b; Momozu et al., 2003; Oida et al., 1999, 2002; Nakashima and Oida, 2004). However, some drawbacks have also been pointed out in this method. Since the original DEM theory treated the analyzed object as an assembly of discontinuous elements, this method should be improved for the analysis of soil-tool interactions such as those occurring during cutting and fracturing for cohesive soil.

The modification of constitutive models associated with the DEM has been carried out by some researchers in order to effectively implement them in their study. For example, in the field of civil engineering, the DEM model was extended to simulate dynamic cliff collapse (Iwashita and Hakuno, 1990). In the field of terramechanics, Momozu et al. (2003) developed a modified DEM model which considered the effect of adhesion, and applied it to the soil cutting process performed by a simple cutting tool. The result of the simulation satisfactorily represented the soil separation resulting from the motion of the blade.

Although the DEM is a promising method for simulating soil-tool interaction, there are few reports on the improvement of this method for application to the field of agricultural machinery. This research article describes an improved DEM model for simulating the soil loosening process and discusses its applicability to the interaction between the soil and the subsoiler shank.

2. MATERIALS AND METHODS

2.1 Procedure of the Field Experiment

In order to examine the effect of subsoiling, an experiment was carried out as a full-scale test at the field belonging to the National Agricultural Research Center for Western Region, Kagawa, Japan. The working width and depth were set to be 140 cm and 30 cm, respectively. Figure 2 shows a view of the field experiment. In order to mark the cracks in the soil layer, white paint was poured into them after subsoiling. Three days later, the field was excavated by using a backhoe, and the features of cracking, such as the failure planes and failure zones, were examined. The soil profile for the examination was set to be perpendicular to the direction of tool travel. In order to validate the numerical simulation, three types of shank arrangements were provided for comparison, as shown in Figure 3. The soil properties, the conditions of the test field, and the working conditions of the subsoiler are listed in Table 1.



Figure 2. View of the field experiment.

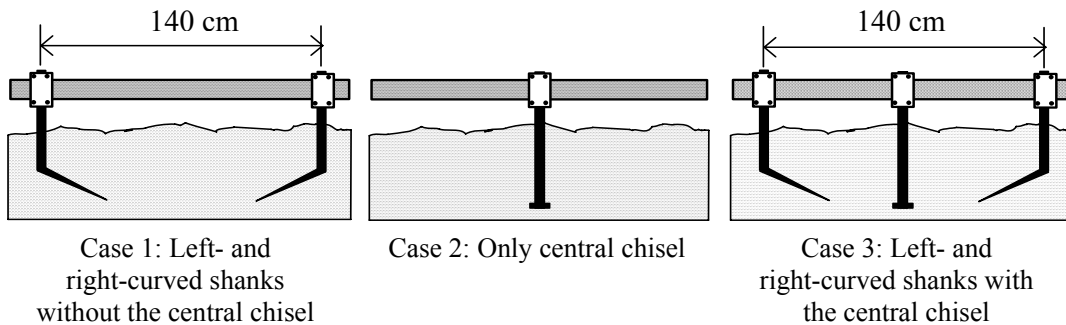


Figure 3. Shank arrangement on the subsoiler provided in the field experiment.

Table 1. Soil properties, field conditions, and working conditions of the subsoiler.

Soil properties		
Composition	Sand (20-2000 µm)	58.9 %
	Silt (2-20 µm)	18.4 %
	Clay (< 2 µm)	22.7 %
Soil type		
Consistency		SCL
Liquid limit		41.2 %
Plastic limit		26.6 %
Field conditions		
Moisture content		13.3 %
Soil wet density		2.0 g/cm ³
Internal friction angle		50.9 °
Cohesion		54.9 kPa
Soil strength*	(5-cm depth)	2.5 Mpa
	(15-cm depth)	4.2 Mpa
	(25-cm depth)	4.1 Mpa
	(35-cm depth)	4.6 Mpa
Working conditions of the subsoiler		
Working width		140 cm
Working depth		30 cm
Working speed		0.15 m/s
Vibration frequency		13 Hz
Vibration amplitude		0.3-1.3 cm

*Measured with Yamanaka soil hardness tester

2.2 Preparing the Virtual Soil Bin by DEM

In order to simulate the soil loosening process caused by the subsoiler, a numerical model using the DEM was developed. As the DEM model is a two-dimensional model, the analyzed

cross-sectional area was assumed to be the same as that in the field experiment. As shown in Figure 4, a virtual soil bin 160 cm wide and 40 cm deep was prepared. The diameters of the elements were set as 0.8 and 0.7 cm considering the number of elements and computation power, and the analyzed area consisted of 13,167 elements.

The subsoiler shank moved up and down in this virtual soil bin. Three types of shank arrangements which corresponded to those in the field experiment were provided. However, as for the central shank, only the chisel was presented because the central shank would act as a “wall” in this two-dimensional analyzing area and the force transmission from left to right over the central shank would not be achieved. The working width, working depth and the vibration frequency of the shank were set to be 140 cm, 30 cm and 13 Hz, respectively; these values were identical to those in the field experiment. The amplitude of the shank vibration was assumed to be 0.5 cm which was within the range of that in the field experiment.

In this study, to prevent the elements beneath the shanks were compressed, the vibration of the shank started at the position of -0.5 cm. The vibration time of the shank was set to be 1.0 s because the width of the shank was 15.0 cm and the traveling speed of the subsoiler in the field experiment was 15.0 cm/s. The shank movement ended at the position of -0.5 cm after vibrating for 1.0 s, and the simulation continued up to 1.3 s in order to settle the movement of elements. However, in case that the curved shanks and central chisel were present, vibration of central chisel started after the curved shanks’ movement ended (namely, the elapsed time of 1.0 s) because the central chisel traveled behind the curved shanks as shown in Figure 1. In this case, total elapsed time was 2.3 s.

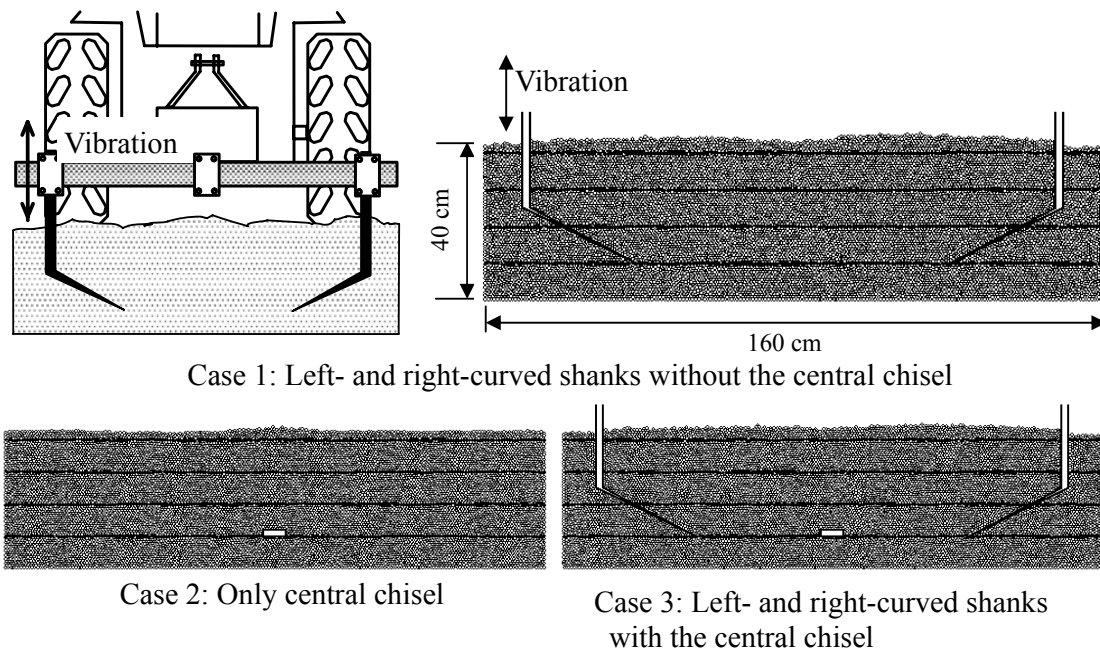


Figure 4. Virtual soil bin and shank arrangements in the DEM simulation.

2.3 Improvement of Mechanical Relationships between Elements for Continuity of Soil

H. Tanaka, A. Oida, M. Daikoku, K. Inooku, O. Sumikawa, Y. Nagasaki and M. Miyazaki. “DEM Simulation of Soil Loosening Process Caused by a Vibrating Subsoiler”. Agricultural Engineering International: the CIGR Ejournal. Manuscript PM 05 010. Vol. IX. November, 2007.

In the conventional DEM model, the elements are perfectly discontinuous with each other, which is suitable for the analysis of grain or sand. On the other hand, this study treats the soil fracture caused by the subsoiler shank movement. In this case, the soil layer is usually hard and continuous. Therefore, based on the concept of the extended DEM (Iwashita and Hakuno, 1990), the mechanical relationships between the elements are improved in terms of the continuity of the soil.

In order to consider the continuity of the soil, a special cycle is included in the program before the determination of the soil-tool interaction. In this cycle, spring and dashpot in tension are installed along with no-compression joint between all the contacting elements, as shown in Figure 5. This operation means that the contacting elements are connected with each other at contact points and the normal force between the elements acts both in the compressive and tensile directions. In other words, the analyzed area behaves as a continuum rather than as an assembly of discontinuous elements in the initial stage of the simulation. This connection is maintained in the later cycles of calculation unless the mechanical situation between elements satisfies the failure criteria. The failure criterion in the normal direction is defined as the tensile failure which depends on the limit of connection for the tension spring between the connected elements. Using a coefficient for tensile failure d_c , the limit of connection for the tension spring is given as follows:

$$-d_c(r_i + r_j) \leq r_i + r_j - r_{ij} \quad (1)$$

where, r_i is the radius of element i; r_j , the radius of element j; and r_{ij} , the distance between the centers of elements i and j. The term $r_i + r_j - r_{ij}$ shows the magnitude of overlap for the elements i and j, as shown in Figure 6. The characteristics of the springs during compression and tension are shown in Figure 7, and the contact modes of the connected elements in the normal direction are shown in Figure 8. The state of connection is illustrated by drawing a line between the centers of the connected elements and it enables a good understanding of the soil loosening, as shown in Figure 9. The failure criterion in the tangential direction is given by Coulomb's law. The details of the calculations for the forces and the detection of tensile and sliding failures for the connected elements are described in the next section.

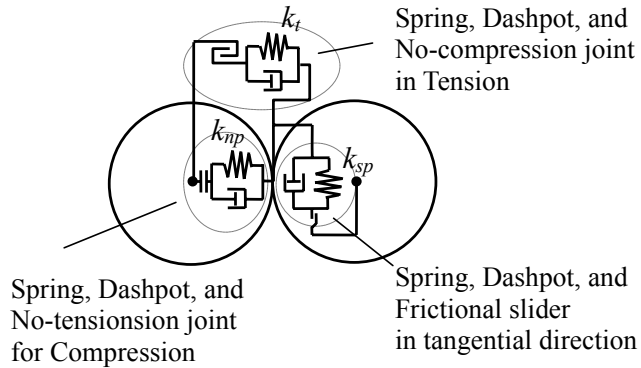


Figure 5. Improved mechanical relationships between elements.

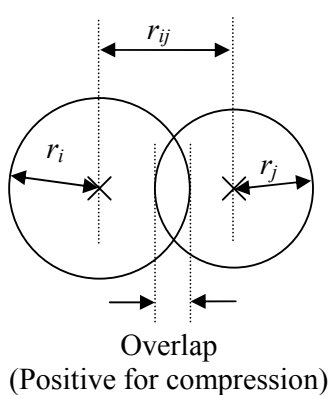


Figure 6. Definition of overlap.

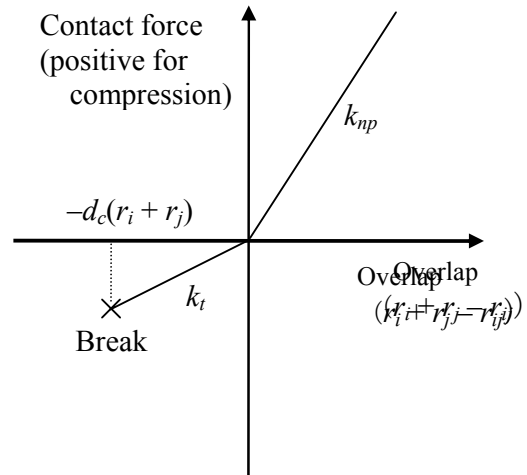


Figure 7. Characteristics of normal springs.

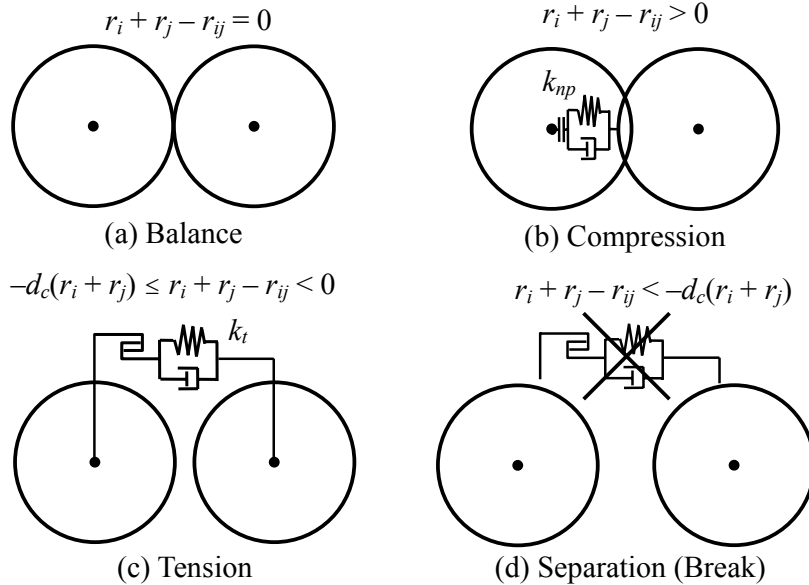


Figure 8. Contact mode and failure criterion in the normal direction for connected elements.

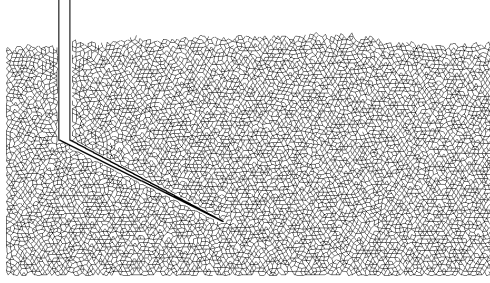


Figure 9. State of connection between elements.

2.4 DEM Formulation for Analysis of Cracking

The conventional DEM theory and formulations were described in a previous paper (Tanaka et al., 2000). In this section, the procedure for the determination of the contact forces and the detection of tensile and sliding failures in the improved model is described. In the original DEM theory, the normal force is calculated as the compressive force. On the other hand, in the present research, the normal force acts both in the compressive and tensile directions between the connected elements.

If $r_i + r_j - r_{ij} > 0$, a compressive force (namely, a repulsive force) is generated between the connected elements and it is given as follows.

$$[f_n]_t = [e_n]_t + [d_n]_t = k_{np}(r_i + r_j - r_{ij}) + [d_n]_t \quad (2)$$

Here, $[f_n]_t$ is the normal force on the element; $[e_n]_t$ and $[d_n]_t$, the spring and damping forces acting on the element; and k_{np} , the spring constant for the compressive force. The subscript t means “at the time t ” in the simulation.

In the case of $r_i + r_j - r_{ij} \leq 0$, a tensile force is generated between the elements, and it is given by the following equation.

$$[f_n]_t = [e_n]_t + [d_n]_t = k_t(r_i + r_j - r_{ij}) + [d_n]_t \quad (3)$$

Here, k_t is the spring constant for the tensile force. In the tangential direction, the contact force $[f_s]_t$ is estimated as the sum of the spring force $[e_s]_t$ and damping force $[d_s]_t$ as follows.

$$[f_s]_t = [e_s]_t + [d_s]_t \quad (4)$$

Here, the critical force in the tangential direction is defined. In this study, Coulomb's law is applied. When the normal force acts as a compressive force (Fig. 7 (b)), the critical tangential force is the sum of the frictional force and cohesive force, as shown in eq. (5). On the other hand, the critical tangential force equals the cohesive force, as shown in eq. (6), when the normal force acts as a tensile force (Fig. 7 (c)).

$$[e_s]_t \leq [e_n]_t \tan \phi + C \quad (5)$$

$$[e_s]_t \leq C \quad (6)$$

Here, ϕ is the internal friction angle of the soil, and C is the cohesive force calculated from the cohesion c .

The fracturing of a soil layer is achieved when the connection between the connected

elements (namely, the spring in tension) is broken. There are three classification factors that must be examined for detecting the breaking.

In the first case, the connection between the connected elements is broken due to tensile failure in the normal direction. The detection of the breaking depends on the critical condition for the magnitude of overlap for the connected elements i and j as shown in eq. (1). Therefore, in the case of $r_i + r_j - r_{ij} < -d_c(r_i + r_j)$, it follows that a tension crack occurs and the contact forces are not generated between the elements. In this case, the contact forces $[f_n]_t$ and $[f_s]_t$ are calculated by using eqs. (7) and (8) instead of eqs. (3) and (4), respectively.

$$[f_n]_t = 0 \quad (7)$$

$$[f_s]_t = 0 \quad (8)$$

In the second case, a sliding failure occurs between the connected elements, while the compressive force acts in the normal direction. This case depends on the critical condition relating to the tangential spring force, as shown in eq. (5).

Therefore, if $||[e_s]_t| > [e_n]_t \tan \phi + C$, the tangential force $[f_s]_t$ is calculated by using eq. (9) instead of eq. (4).

$$[f_s]_t = [e_n]_t \tan \phi \operatorname{sig}[[e_s]_t] \quad (9)$$

Here, $\operatorname{sig}[[e_s]_t]$ is the sign of $[e_s]_t$. This equation indicates that a crack is generated between the elements, but the elements are still in contact with each other. In this case, the cohesion loses its effect, but the frictional force remains in the tangential direction. The calculation of the contacting force in the normal direction continues to be performed by using eq. (2).

In the third case, the sliding failure occurs between the connected elements, while the tensile force acts in the normal direction. This case depends on the critical condition, as shown in eq. (6). Therefore, if $[e_s]_t > C$, the calculations of the contacting forces $[f_n]_t$ and $[f_s]_t$ are performed by eqs. (7) and (8) instead of eqs. (3) and (4), respectively. This operation implies that the contact forces are generated neither in the normal direction nor in the tangential direction because a crack is generated and the elements are separated from each other.

These judgments are performed for all the connected elements at each step of the calculation. Once the connection between the connected elements is broken, the spring and dashpot in tension are no longer effective in the later cycle of the calculation. In such a case, only the compressive force obtained from eq. (2) is applied in the normal direction. In the tangential direction, as the effect of the cohesion between the elements is considered to be lost, only frictional force is generated between the contacting elements. Therefore, the critical condition for the spring force in the tangential direction is expressed by the following equation instead of eq. (5).

$$[e_s]_t \leq [e_n]_t \tan \phi \quad (10)$$

Equations (2) and (10) are the same as those in the conventional DEM formulation. In this way, an improved DEM model is formulated for the analysis of the loosening process of continuous soil. The algorithm for determining the failure and the force between the connected elements is shown in Figure 10 as a flow chart.

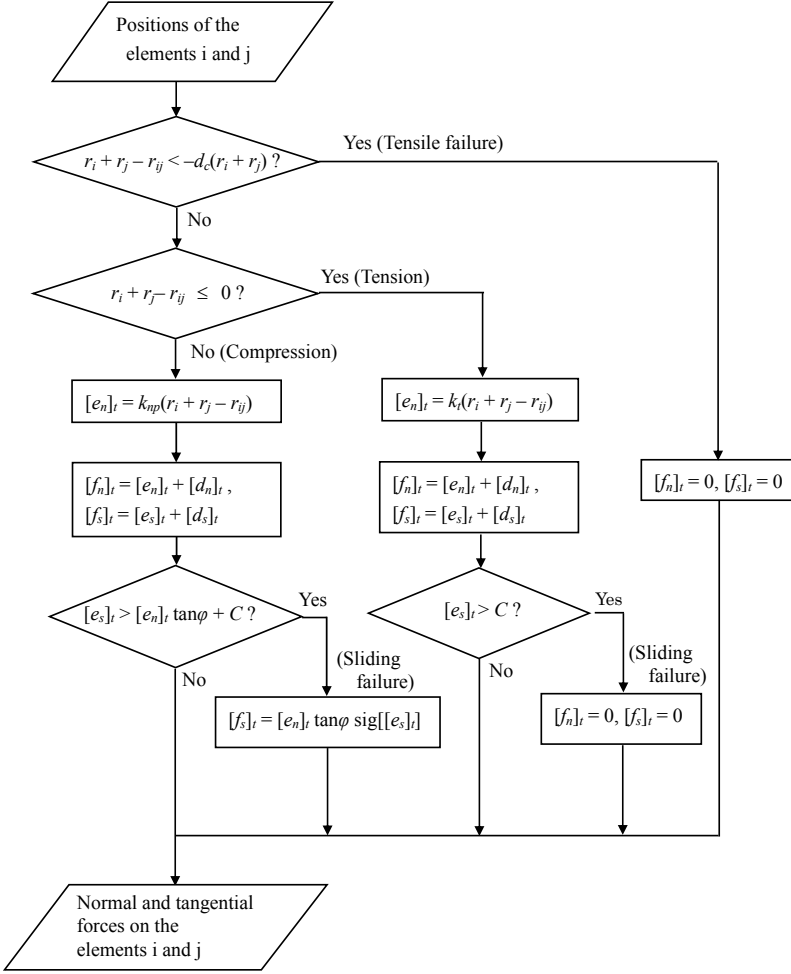


Figure 10. Determination of failure and force between connected elements.

2.5 DEM Parameters

As many reports have mentioned, the concrete method to determine the values of DEM parameters have not been established yet. Therefore, we should make some assumptions and take a trial-and-error method in determining them. In this section, a procedure for determining the values of the DEM parameters in this study is described.

For the spring constants k_{np} , k_{sp} and k_t , certain ratios between them were assumed. The spring constant in the tangential direction k_{sp} should be smaller than that in the normal direction in terms of the stability of solution (Kiyama and Fujimura, 1983). Therefore, in this study, k_{sp} was set to be 0.1 times the k_{np} . As for k_t , the value within the range of $0.5k_{np}$ - $0.75k_{np}$ was considered because soil tensile strength is smaller than its compressive strength. The value of k_{np} was determined as 9.0×10^5 N/m, which referred to the past work (Tanaka et al., 1999); a bending test was performed using an undisturbed soil sample with a rectangular prism of $15 \times 5 \times 5$ cm and $k = 3.0 \times 10^5$ N/m was obtained.

The internal friction angle of soil ϕ , which was measured in the field experiment, was used as the friction angle between the elements in the simulation. The cohesive force C [N] for the simulation was calculated from the cohesion c [kPa] in the field experiment. Considering a certain plane between the contacting elements with the area of $a \times b$ as shown in Figure 11, the cohesive force C was calculated as $cab \times 10^{-1}$. Here, the thickness of the element a was assumed to be 15 cm which was identical to the width of shank, and the b was set as 0.8 cm that was the element's diameter d_1 .

The diameters of the elements d_1 and d_2 were determined as 0.8 and 0.7 cm, respectively, by considering the computer power. The mass of each element was calculated using the diameter, thickness and density of the element. The density of the element was 2.0 g/cm³ which was equal to the soil wet density in the field experiment. Thickness of the element was 15 cm as mentioned above. Then, the masses of the elements m_1 and m_2 were estimated as 15.1 and 11.5 g, respectively. However, these values required correction to fit the experimental results. The settled values of m_1 and m_2 were 30.2 and 23.0 g, respectively.

The viscous damping coefficient η for each spring-dashpot system was calculated as $\sqrt{2m_2 k}$. When η is taken as $\sqrt{2m_2 k}$, the critical time step of the calculation for the stability of solution is given by using the following inequality in which energy dissipation between contacting elements was take into account (Tanaka et. al., 1998). The value of time step was determined within this range.

$$\Delta t < 0.465 \sqrt{m_2 / k_{np}} \quad (11)$$

In this manner, the values of the DEM parameters were estimated. However, these values were tentative and required some corrections by trial-and-error method. The settled values were obtained by comparing the results of simulation with those of the field experiment. The set of values of DEM parameters used in this study are listed in Table 2.

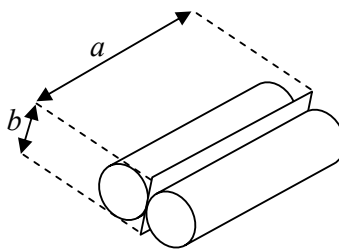


Figure 11. A plane for determination of cohesive force C .

Table 2. DEM parameters used in the simulation

Parameters	Values		Remarks
Normal spring constant for compressive force between elements (k_{np}):	9.0×10^5	[N/m]	Referring to a past work and trial-and-error.
Normal spring constant for tensile force between elements (k_t):	6.75×10^5	[N/m]	Trial-and-error with $(0.5 \sim 0.75)k_{np}$, and settled in $0.75k_{np}$.
Tangential spring constant between elements (k_{sp}):	9.0×10^4	[N/m]	Stability of solution, $0.1k_{np}$.
Cohesive force between connecting elements (C):	65.9	[N]	Calculated from cohesion c in the field experiment.
Internal friction angle between elements (ϕ):	50.9	[°]	Measured value in the field experiment.
Coefficient for tensile failure (d_c):	0.005	[-]	Trial-and-error with $0.001 \sim 0.05$, and settled in 0.005.
Thickness of the element (a):	15.0	[cm]	Width of shank.
Density of the element:	2.0	[g/cm ³]	Soil wet density in the field experiment.
Diameters of elements (d_1, d_2):	0.8, 0.7	[cm]	Considering the number of elements and computational power.
Mass of elements (m_1, m_2):	30.2, 23.0	[g]	Calculated from diameters, thickness and density of elements, and corrected.
Time step of the calculation (Δt):	4.0×10^{-5}	[s]	Stability of solution.

3. RESULTS AND DISCUSSION

3.1 Result of the Field Experiment and Calibration of the DEM Parameters

Figure 12 shows the original image of the field cross section after subsoiling. It shows the result of subsoiling when two curved shanks are applied. It was observed that cracks were generated at the tip of each shank and these cracks progressed diagonally on the ground surface. The crack indicates the failure plane in the lateral direction of tool travel. The failure zone is distinctly recognized as the area that is enclosed by the failure plane and the tracks of the shank. Moreover, in the failure zone, many cracks are generated and the soil layer is fractured into blocks. The area outside the failure zone does not seem to be disturbed.

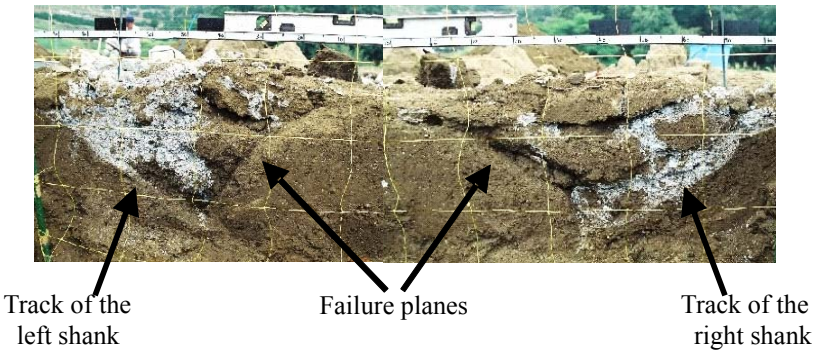


Figure 12. Cracking in the cross section of the field.

As mentioned above, a concrete method to determine the values of the DEM parameters has not been established yet. Therefore, we should seek an appropriate set of values for the DEM parameters by using the trial-and-error method in order to suit the results of the field experiment. As an example of the calibration of the parameter, simulation results with different values of d_c are shown in Figure 13. These figures show the results for an elapsed time of 1.3 s. When we considered the values of d_c as 0.001 and 0.003, almost all the springs above the shank were broken and the soil fracture was very prominent. On the other hand, when we considered the values of d_c as 0.01, 0.02, and 0.05, we could observe cracks in the soil layer; however, the soil fracture in the failure zone could not be observed. When we considered d_c as 0.005, we could find both the failure plane and soil fracture in the failure zone, and the macroscopic observations agreed with the results of the abovementioned field experiment. Therefore, we considered the value of d_c as 0.005 for obtaining a reasonable simulation result.

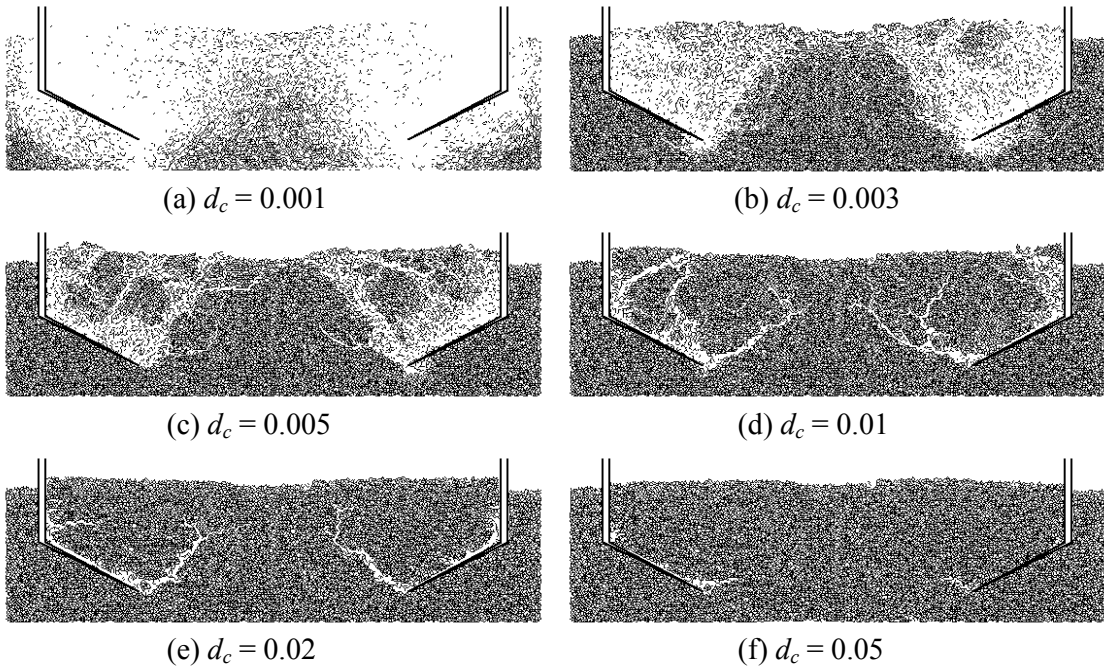


Figure 13. Simulation results with different values of d_c .

Figure 14 indicates the transition of the state of connection between the elements when we consider d_c as 0.005. In the initial stage of the simulation, almost all the elements were connected with each other. As the simulation progressed, a crack was generated at the tip of each shank. The cracks progressed diagonally on the ground surface, and the failure zones above the shanks were appeared. The elements in the failure zones moved up and down following the motion of the shank. The contours of the failure zones qualitatively corresponded to those observed in the field experiment. The simulation result also supported the fact that the area outside the failure zone was not disturbed. Moreover, the connections between elements were broken one after another in the failure zone. Those results indicate that we can assess the dynamic behavior of the soil loosening process and the distribution of cracking in the subsurface layer, which are usually hard to observe, by using this method.

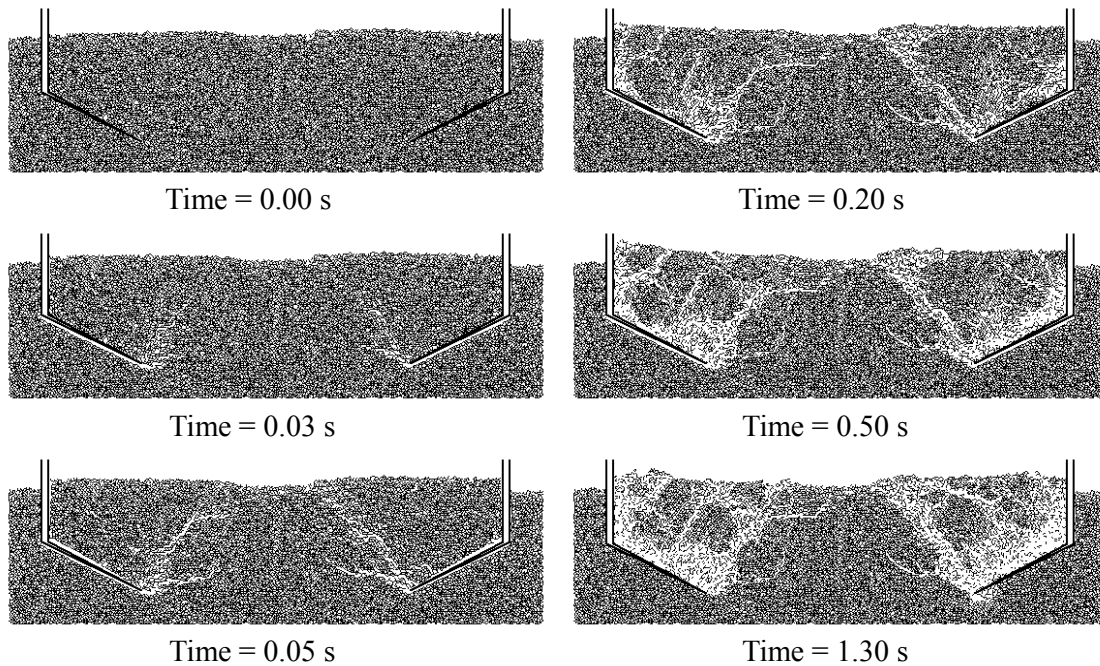


Figure 14. Cracking and fracturing of soil layer as revealed in DEM simulation.

3.2 Validation of the Model and Parameters for Different Shank Arrangements

Figures 15(a) and (b) show the results of the field experiment and those of the DEM simulation obtained by using the values of the parameters listed in Table 2 for different shank arrangements. Figure 15(a) shows the result when only the center chisel was present. Figure 15(b) shows the result when both the curved shanks and center chisel were used. In both cases, the characteristics of soil fracture according to the result of the simulation qualitatively agreed with those obtained from the field experiment. From these results, it is confirmed that once we set proper values for the DEM parameters for a soil condition, the profile of the soil failure that depends on the shank's geometry can be satisfactorily simulated under the same soil condition.

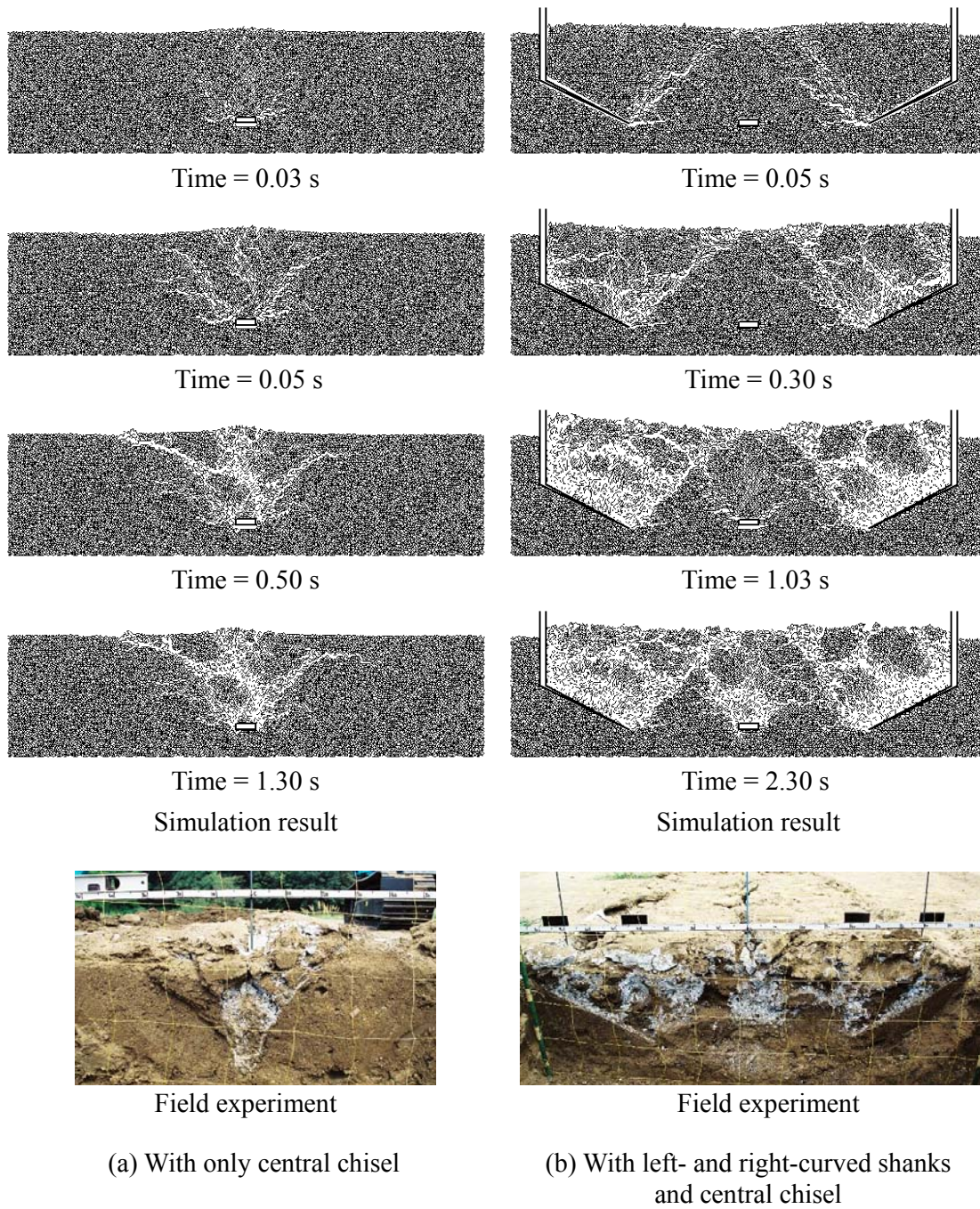


Figure 15. Soil fracture in the results of DEM simulation and field experiment for different shank arrangements.

4. CONCLUSIONS

In order to simulate the soil loosening process caused by the subsoiler shank, a numerical model was developed by means of the DEM. As the original DEM treats the object as an assembly of discontinuous elements, mechanical relationships between the elements were improved. By introducing a spring for representing the tension between the elements, the continuity of the soil layer and its cracking caused by the motion of subsoiler shanks could be represented. The simulation results were in good agreement with the field experiment results as macroscopic behavior, when we set appropriate values for the DEM parameters in the improved DEM model. It is also indicated that we can estimate not only the failure plane but also the distribution of cracking in the failure zone by this simulation method. In the near future, this method is expected to provide considerable information for the improvement of the characteristics of such implements, such as the shape of the shank and the manner of arranging the shank.

For further study, large-scale analysis using a large number of elements with smaller diameters should be performed to obtain more detailed information related to the dynamic problems of soil-machine interaction; and the method to determine the values of DEM parameters depending on the soil mechanical properties should also be established.

5. ACKNOWLEDGEMENTS

The authors express their warm gratitude to A. Prof. Dr. Eiichiro Sakaguchi, A. Prof. Dr. Hiroshi Nakashima, and Dr. Masatoshi Momozu for their assistance in developing the simulation program, and to Mr. Masuhiro Fujikawa, Mr. Koji Seki, Mr. Takefumi Matsuzaki, Mr. Jiro Takao, and Mr. Yasufumi Otani for their assistance in the experimental studies. The authors also thank Kawabe Noken Sangyo Co., Ltd. for providing the test subsoiler.

6. REFERENCES

- Cundall, P. A. and O. D. L. Strack. 1979. A discrete numerical method for granular assemblies. *Geotechnique* 29(1): 47–65.
- Iwashita, K. and M. Hakuno. 1990. Modified distinct element method simulation of dynamic cliff collapse. *Structural Eng./Earthquake Eng., JSCE* 7(1): 133–142.
- Kiyama, H. and H. Fujimura. 1983. Application of cundall's discrete block method to gravity flow analysis of rock-like granular materials. *Proc. JSCE* 333:137–146 (In Japanese).
- Momozu, M., A. Oida, M. Yamazaki and A. J. Koolen. 2003. Simulation of a soil loosening process by means of the modified distinct element method. *J. Terramechanics* 39(4): 207–20.
- Nakashima, H. and A. Oida. 2004. Algorithm and implementation of soil-tire contact analysis

H. Tanaka, A. Oida, M. Daikoku, K. Inooku, O. Sumikawa, Y. Nagasaki and M. Miyazaki. “DEM Simulation of Soil Loosening Process Caused by a Vibrating Subsoiler”. Agricultural Engineering International: the CIGR Ejournal. Manuscript PM 05 010. Vol. IX. November, 2007.

- code based on dynamic FE-DE method. *J. Terramechanics* 41(2–3): 127–37.
- Oida, A., S. Ohkubo and H. Schwanghart. 1999. Effect of tire lug cross section on tire performance simulated by distinct element method. In *Proc. of the 13th Int. Conf. of ISTVS*, Munich, Germany, 345–352. September.
- Oida, A. and M. Momozu. 2002. Simulation of soil behavior and reaction by machine part by means of DEM. *Agricultural Engineering International: the CIGR Ejournal of Scientific Research and Development* PM 01 004 Vol. IV: 1–7.
- Sakaguchi, E., et. al. 2001. Numerical simulation of the shaking separation of paddy and brown rice using the discrete element method. *J. Agric. Engng. Res.* 79(3): 307–15.
- Tanaka, H., et. al. 1998. A study on the stability of solution in the distinct element method. *J. Soc. Powder Technology, Japan* 35(3):19–27 (In Japanese).
- Tanaka, H., et. al. 1999. Numerical analysis of soil loosening in subsurface tillage by a vibrating type subsoiler by means of the distinct element method. In *Proc. of the 13th Int. Conf. of ISTVS*, Munich, Germany, 791–798. September.
- Tanaka, H., M. Momozu, A. Oida and M. Yamazaki. 2000a. Simulation of soil deformation and resistance at bar penetration by the distinct element method. *J. Terramechanics* 37(1): 41–56.
- Tanaka, H., K. Inooku, Y. Nagasaki, M. Miyazaki, O. Sumikawa and A. Oida. 2000b. Simulation of soil loosening at subsurface tillage using a vibrating type subsoiler by means of the Distinct Element Method. In *Proc. 8th European ISTVS Conf.*, Umea, Sweden, 32–38. June.